Gulf Journal of Mathematics
Vol 16, Issue 2 (2024) 278-290

ISSN: 2309-4966
https://doi.org/10.56947/gjom.v16i2.1815

EFFECTS OF DIFFERENT NANOPARTICLES ON THE TWO IMMISCIBLE LIQUIDS FLOW IN AN INCLINED CHANNEL WITH JOULE HEATING AND VISCOUS DISSIPATION

M. PADMA DEVI[1], KOMAL GOYAL[2], S. SRINIVAS[2*], B. SATYANARAYANA[2]

ABSTRACT. The problem of magnetohydrodynamics of immiscible liquid flow in a channel having inclined orientation with porous space and different types of nanoparticles has been investigated. The channel is separated into two regions. The lower region is filled with Al_2O_3-water, and the upper region is occupied by Cu-water. The governing equations are numerically solved using R-K 4th-order with a shooting technique to highlight the effect of the magnetic field parameter, Grashof number, inclination angle, viscous dissipation, and the ratio of permeability of two regions. As the Hartmann number increases, there are two regions where the fluid's temperature and velocity decrease. The effects of different nanoparticle combinations on flow variables have also been discussed. Tabulated numerical data for the distribution of shear stress are provided for a range of physical parameters.

1. INTRODUCTION

Concentration recovery, purification of organophilic solutes (such as amino acids), and solvent extraction all require knowledge of incompressible, non-miscible liquid flow. In all of these applications, the thermal conductivity of liquid plays a crucial role in developing energy-efficient heat industries. As a result, heat carrier fluids are used in heat transfer systems. Moreover, those heat transfer models can be used in a variety of industries as well, including paper production, petrochemicals, processing plants, chemicals, foods, and hydronic heating and cooling systems in buildings. Although there have been many studies on fluid heat transfer, there is still a need to improve with a superior thermal conductivity than the existing ones so that they can be used in real-life applications to enhance heat transfer [10].

Researchers have explored a new class of liquid known as "nanofluid", which are made of suspensions of solid particles of diameters less than 2 micrometres, as seen in Das and Choi [5]. Choi and Eastman [3] studied that suspending metallic nanoparticles can produce heat transfer fluid with better thermal characteristics

Date: Received: Feb 11, 2024; Accepted: Mar 17, 2024

* Corresponding author: S. Srinivas.

2020 *Mathematics Subject Classification.* Primary 46L55; Secondary 44B20.

Key words and phrases. Different Nanoparticles, Viscous dissipiation, Darcy dissipation, Joule heating.

than base fluids. Eastman et al. [6] examined the synthesis, suspension characteristics, and heat transfer behaviour of fluids containing nanocrystalline aluminium, copper oxide, and copper. When compared to the thermal conductivity of base fluids, which are commonly used for heat transfer, such as ethylene glycol and water, have comparatively lower thermal conductivities than the nanofluid. Those nanoparticles have a high heat conductivity, which can improve the thermal conductivity of the base liquid. Because of the wide range of applications for immiscible nanoliquid flow, various intriguing studies on the effect of nanoparticles on the flow of fluids and thermal properties can be seen in the literature, such as [3, 4, 11] and references therein.

The impact of magnetic fields has several applications in chemical and industrial engineering. When an electrically conductive fluid comes into contact with a magnetic field, it can affect industrial equipment such as generators and magnetohydrodynamic (MHD) control of the boundary layer. Sheikholeslami et al. [16] researched the impacts of a magnetic field on heat transfer and flow field of CuO-water nanoliquid in a heated enclosure. Malvandi et al. [13] explored the impact of a magnetic field on mixed convection in a vertical annulus filled with water as base fluid with the suspension of aluminium oxide nanoparticles.

The effect of ohmic heating on the flow phenomena is important for many practical and industrial uses. It is also applicable to equipment used in food preparation. The study conducted by Evenhuis and Haddad [7] examines how electrical energy, when passed through an electrically resistant food item, transforms into thermal energy and generates heat within the food. Ur Rasheed et al. [18] investigated the effects of ohmic heating, viscous dissipation, and heat generation on MHD liquid flow. The effects of ohmic heating and viscous dissipation on MHD flow over an elastic surface immersed in a porous space were examined by Swain et al. [17].

The literature has a significant amount of study on porous media due to the fact that it is useful in a variety of scientific fields. A number of researchers have shown an interest in the flow of porous surfaces in the last few decades. The investigation of the transport of liquid via porous media is significant in a variety of engineering domains as well, including geothermal and medicinal research. An investigation was conducted by Abbas et al. [1] to examine the impact of the Darcy-Forchheimer relation on third-grade liquid flow over an inclined stretched sheet that was embedded in a porous media. Nield and Kuznetsov [12] investigated the convection of heat transport in a porous media saturated with nanoliquid.

To the best of our knowledge, the investigation pertaining to the influence of viscous dissipation, ohmic heating, and thermal radiation on two-layered immiscible nanofluid flow has not been presented in the literature. Hence, the current study explores the impact of pulsatile pressure gradient on layered non-miscible nanofluid flow filled with porous space in an inclined channel. Studies of this sort are helpful in various industrial and geothermal applications [9, 19]. The effect of pertinent parameters such as angle of inclination, liquid width parameter, and Eckert number on the flow field and temperature distribution has been numerically evaluated using the Runge-Kutta 4th-order approach together with

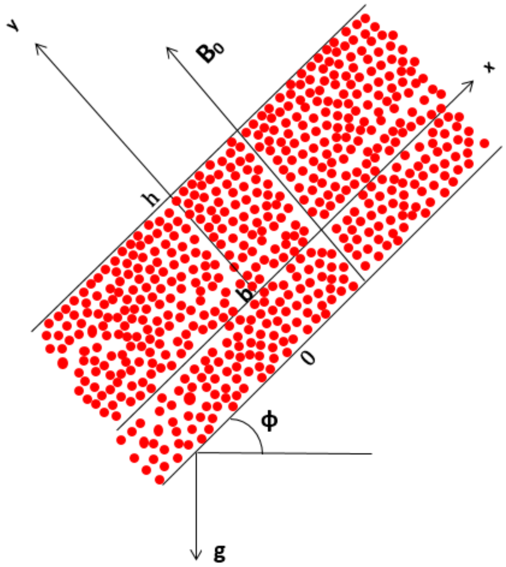

FIGURE 1. Flow geometry

the shooting technique. Moreover, the impact of the Hartmann and Darcy numbers on stress distribution is presented in tabular form on both the walls of the channel.

2. Formulation of the problem

The effects of MHD on two layered immiscible nanofluid flow with different nanoparticles in an inclined channel are investigated. The geometry of the model is illustrated in Fig. 1. The flow is chosen along the x-direction and the y-axis is perpendicular to the channel walls. Flow is divided into two portions, region-I from $0 \leq y \leq b$ and region-II from $b \leq y \leq h$. Both regions of the channel are occupied by Al_2O_3 and Cu as nanoparticles with varying densities, ρ_{1nf}, ρ_{2nf}, two distinct viscosities μ_{1nf}, μ_{2nf}, and electrical conductivities σ_{1nf}, σ_{2nf}, respectively. The fluid is considered to be injected into the channel with the velocity v_0 through the injection wall at $y = 0$ and sucked out with the same velocity v_0 through the suction wall at $y = h$. A uniform magnetic field of intensity B_0 is applied perpendicular to the walls. The influence of porous medium's permeability, viscous dissipation, Darcy dissipation, magnetic dissipation, and thermal radiation has been considered.

The following governing equations are (See Refs [2, 8]):

Region-I

$$\rho_{1nf}\left(\frac{\partial u_1}{\partial t}+v\frac{\partial u_1}{\partial y}\right)=-\frac{\partial p}{\partial x}+\mu_{1nf}\frac{\partial^2 u_1}{\partial y^2}+\rho_{1nf}g\beta_{1nf}\left(T_1-T_0\right)\sin\phi-\sigma_{1nf}B_0^2u_1-\frac{\mu_{1nf}}{k_{1p}}u_1 \tag{2.1}$$

$$\left(\rho C_p\right)_{1nf}\left(\frac{\partial T_1}{\partial t}+v\frac{\partial T_1}{\partial y}\right)=k_{1nf}\frac{\partial^2 T_1}{\partial y^2}+\mu_{1nf}\left(\frac{\partial u_1}{\partial y}\right)^2-\frac{\partial q_r}{\partial y}-\sigma_{1nf}B_0^2u_1^2+\frac{\mu_{1nf}}{k_{1p}}u_1^2 \tag{2.2}$$

Region-II

$$\rho_{2nf}\left(\frac{\partial u_2}{\partial t}+v\frac{\partial u_2}{\partial y}\right)=-\frac{\partial p}{\partial x}+\mu_{2nf}\frac{\partial^2 u_2}{\partial y^2}+\rho_{2nf}g\beta_{2nf}\left(T_2-T_0\right)\sin\phi-\sigma_{2nf}B_0^2u_2-\frac{\mu_{2nf}}{k_{2p}}u_2 \tag{2.3}$$

$$(\rho C_p)_{2nf}\left(\frac{\partial T_2}{\partial t}+v\frac{\partial T_2}{\partial y}\right)=k_{2nf}\frac{\partial^2 T_2}{\partial y^2}+\mu_{2nf}\left(\frac{\partial u_2}{\partial y}\right)^2-\frac{\partial q_r}{\partial y}-\sigma_{2nf}B_0^2u_2^2+\frac{\mu_{2nf}}{k_{2p}}u_2^2 \tag{2.4}$$

Eqns. 2.1-2.4 are solved by using the boundary conditions, which can be seen in Ref. [9]:

$$\begin{gathered}
u_1^*\left(0\right)=0, u_2^*\left(h\right)=0, u_1^*\left(b\right)=u_2^*\left(b\right),\\
\mu_{1nf}\left.\frac{\partial u_1^*}{\partial y}\right|_{y=b}=\mu_{2nf}\left.\frac{\partial u_2^*}{\partial y}\right|_{y=b}\\
T_1^*\left(0\right)=T_{w_1}, T_2^*\left(h\right)=T_{w_2}, T_1^*\left(b\right)=T_2^*\left(b\right),\\
k_{1nf}\left.\frac{\partial T_1^*}{\partial y}\right|_{y=b}=k_{2nf}\left.\frac{\partial T_2^*}{\partial y}\right|_{y=b}
\end{gathered} \tag{2.5}$$

The non-dimensional quantities are given below:-
$x=\dfrac{x^*}{h}$, $y=\dfrac{y^*}{h}$, $b=\dfrac{b^*}{h}$, $u_i=\dfrac{u_i^*w}{A}$, $t=t^*w$, $P=\dfrac{P^*}{A\rho_{1f}h}$, $H=h\sqrt{\dfrac{w}{\nu_{1f}}}$, $R=\dfrac{\nu_0 h}{\nu_{1f}}$, $u_{i1}=\dfrac{u_{i1}^*w}{A}$, $u_{i2}=\dfrac{u_{i2}^*w}{A}$ $\alpha_{nf}=\dfrac{\rho_{1nf}}{\rho_{2nf}}$, $A_1=\dfrac{\rho_{1nf}}{\rho_{1f}}$, $A_2=\dfrac{\mu_{1nf}}{\mu_{1f}}$, $A_3=\dfrac{(\rho C_p)_{1nf}}{(\rho C_p)_{1f}}$, $A_4=\dfrac{k_{1nf}}{k_{1f}}$, $A_5=\dfrac{\sigma_{1nf}}{\sigma_{1f}}$, $M_1=B_0h\sqrt{\dfrac{\sigma_{1nf}}{\mu_{1f}}}$, $M_2=B_0h\sqrt{\dfrac{\sigma_{2nf}}{\mu_{2f}}}\left(M_2=M_1\sqrt{\dfrac{\beta_nf}{\gamma_nf}}\right)$, $\Pr=\dfrac{\mu_1f}{k_1f}Cp_{1f}$, $Rd=\dfrac{4\sigma^*}{k^*k_{1f}}T_1^3$, $\beta_{nf}=\dfrac{\mu_{1nf}}{\mu_{2nf}}$, $\gamma_{nf}=\dfrac{\sigma_{1nf}}{\sigma_{2nf}}$, $k_{nf}=\dfrac{k_{2nf}}{k_{1nf}}$, $\theta_i=\dfrac{T_i^*-T_0}{T_{w_2}-T_{w_1}}$, $D_a=\dfrac{k_{1p}}{h^2}$, $k_p=\dfrac{k_{2p}}{k_{1p}}$, $Ec=\dfrac{A^2}{\omega^2(C_p)_{1f}\left(T_{w_1}-T_{w_2}\right)}$, $\mathrm{Re}=\dfrac{\rho_{1f}\omega h}{\mu_{1f}A}$

The dimensionless equations in the respective regions are:-
Region-I

$$A_1\left[H^2\frac{du_1}{dt}+R\frac{du_1}{dy}\right]=-H^2\frac{dp}{dx}+A_2\frac{d^2u_1}{dy^2}+\frac{Gr}{\mathrm{Re}}\sin\phi\theta_1-A_5M_1^2u_1-\frac{A_2}{Da}u_1 \tag{2.6}$$

$$A_3 \Pr\left[H^2\frac{d\theta_1}{dt}+R\frac{d\theta_1}{dy}\right]=\left(A_4+\frac{4}{3}Rd\right)\frac{d^2\theta_1}{dy^2}+A_2 Ec\Pr\left(\frac{du_1}{dy}\right)^2+\left(A_5 Ec\Pr M_1^2+\frac{A_2 Ec\Pr}{Da}\right)u_1^2 \tag{2.7}$$

Region-II

$$A_1\alpha_{nf}\beta_{nf}\left[H^2\frac{du_2}{dt}+R\frac{du_2}{dy}\right]=-H^2\beta_{nf}\frac{dp}{dx}+A_2\frac{d^2u_2}{dy^2}+\frac{Gr}{\mathrm{Re}}\sin\phi\theta_2-A_5M_2^2u_2-\frac{A_2}{Da\ kp}u_2 \tag{2.8}$$

$$A_3(\alpha Cp)_{nf}\Pr\beta_{nf}\left[H^2\frac{d\theta_2}{dt}+R\frac{d\theta_2}{dy}\right]=\left(k_{nf}A_4\beta_{nf}+\frac{4}{3}Rd\beta_{nf}\right)\frac{d^2\theta_2}{dy^2}+A_2Ec\Pr\left(\frac{du_2}{dy}\right)^2+\left(A_5Ec\Pr M_2^2+\frac{A_2Ec\Pr}{kpDa}\right)u_2^2 \tag{2.9}$$

The dimensionless velocity and temperature conditions at the wall with interface are given below:

$$\begin{gathered}u_1(0)=0,u_2(1)=0,u_1(b)=u_2(b)\\ \mu_{1nf}\left.\frac{\partial u_1}{\partial y}\right|_{y=b}=\mu_{2nf}\left.\frac{\partial u_2}{\partial y}\right|_{y=b}\\ \theta_1(0)=0,\theta_2(1)=1,\theta_1(b)=\theta_2(b)\\ k_{1nf}\left.\frac{\partial\theta_1}{\partial y}\right|_{y=b}=k_{2nf}\left.\frac{\partial\theta_2}{\partial y}\right|_{y=b}\end{gathered} \tag{2.10}$$

Using the regular perturbation method, the governing equations eqns. 2.6-2.9, along with boundary conditions eqn. 2.10 can be solved:

$$u_i=u_{i1}+\varepsilon u_{i2}e^{it} \tag{2.11}$$

$$\theta_i=\theta_{i1}+\varepsilon\theta_{i2}e^{it} \tag{2.12}$$

Where, q_r^*=Radiative heat flux , using the Rosseland approximation, $q_r^*=-\frac{4\sigma^*}{3k^*}\frac{\partial T^{*4}}{\partial y^*}$.

Here, $\sigma^*=5.6697\times10^{-8}Wm^{-2}K^{-4}$ represents Stefan -Boltzmann constant and k^*= Rosseland mean absorption coefficient. Expressing T^*as a linear function of T, under the assumption that within the liquid, the variations of temperature are small, we get $T^{*4}\cong 4T_1^3T^*-3T_1^4$. The nanoliquid's effective density is expressed as

$$\rho_{1nf}=(1-\phi)\rho_{1f}+\phi\rho_{1s} \tag{2.13}$$

The nanoliquid dynamic viscosity, heat capacity, effective thermal conductivity and effective electrical conductivity can be expressed using the following relations:

$$\mu_{1nf} = \frac{\mu_{1f}}{(1-\phi)^{2.5}} \tag{2.14}$$

$$(\rho C_p)_{1nf} = (1-\phi)(\rho C_p)_{1f} + \phi(\rho C_p)_{1s} \tag{2.15}$$

$$\frac{k_{1nf}}{k_{1f}} = \frac{k_{1s} + 2k_{1f} - 2\phi(k_{1f} - k_{1s})}{k_{1s} + 2k_{1f} + \phi(k_{1f} - k_{1s})} \tag{2.16}$$

$$\frac{\sigma_{1nf}}{\sigma_{1f}} = 1 + \frac{3\phi\left(\frac{\sigma_{1s}}{\sigma_{1f}} - 1\right)}{\left(\frac{\sigma_{1s}}{\sigma_{1f}} + 2\right) - \left(\frac{\sigma_{1s}}{\sigma_{1f}} - 1\right)\phi} \tag{2.17}$$

$$\frac{k_{1nf}}{k_{1f}} = \frac{(m-1)\phi(k_{1s} - k_{1f}) + k_{1s} - (1-m)k_{1f}}{k_{1s} - (1-m)k_{1f} - \phi(k_{1s} - k_{1f})} \tag{2.18}$$

Where m is the shape factor when the shape factor is m=3, Hamilton Crosser's model is transformed into a Maxwell model.
By using eqns. 2.11-2.12, the dimensionless boundary conditions are as follows:

$$u_{11}(0) = 0, u_{12}(0) = 0, u_{21}(1) = 0, u_{22}(1) = 0, u_{11}(b) = u_{21}(b), u_{12}(b) = u_{22}(b),$$

$$\mu_{1nf} \left.\frac{\partial u_{11}}{\partial y}\right|_{y=b} = \mu_{2nf} \left.\frac{\partial u_{21}}{\partial y}\right|_{y=b}$$

$$\mu_{1nf} \left.\frac{\partial u_{12}}{\partial y}\right|_{y=b} = \mu_{2nf} \left.\frac{\partial u_{22}}{\partial y}\right|_{y=b},$$

$$\theta_{11}(0) = 0, \theta_{12}(0) = 0, \theta_{21}(1) = 1, \theta_{22}(1) = 0, \theta_{11}(b) = \theta_{21}(b), \theta_{12}(b) = \theta_{22}(b)$$

$$\begin{aligned} k_{1nf} \left.\frac{\partial \theta_{11}}{\partial y}\right|_{y=b} &= k_{2nf} \left.\frac{\partial \theta_{21}}{\partial y}\right|_{y=b} \\ k_{1nf} \left.\frac{\partial \theta_{12}}{\partial y}\right|_{y=b} &= k_{2nf} \left.\frac{\partial \theta_{22}}{\partial y}\right|_{y=b} \end{aligned} \tag{2.19}$$

2.1. **Shear stress and Rate of heat transfer.** Skin friction and Nusselt number are two characteristics that are important in engineering applications. The skin friction basically corresponds to the velocity boundary layer, while the Nusselt number corresponds to the heat boundary layer. Shear stress measures the resistance that the surface over which the fluid flows provides due to the fluid's viscosity. The heat transfer rate, a ratio of heat transfer due to conduction over convection, is important. The expressions of skin friction and Nusselt number are as follows [14]:

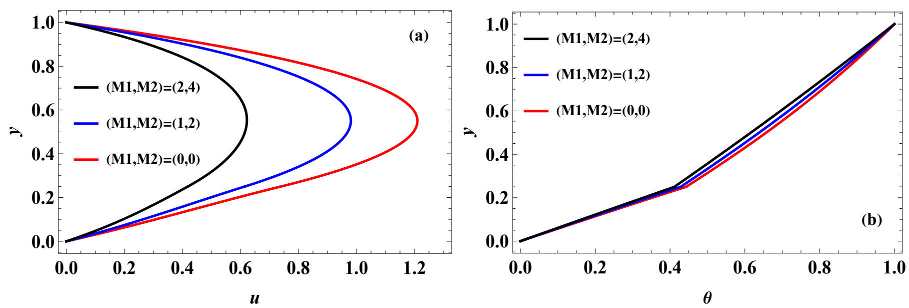

FIGURE 2. Effect of Hartmann number on velocity and temperature profile

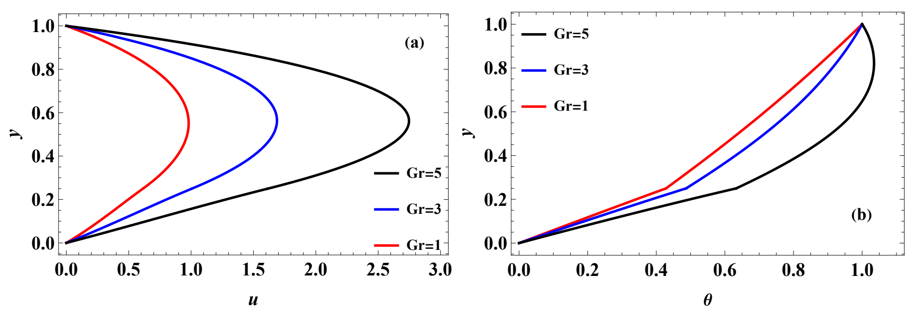

FIGURE 3. Effect of Grashof number on velocity and temperature profile

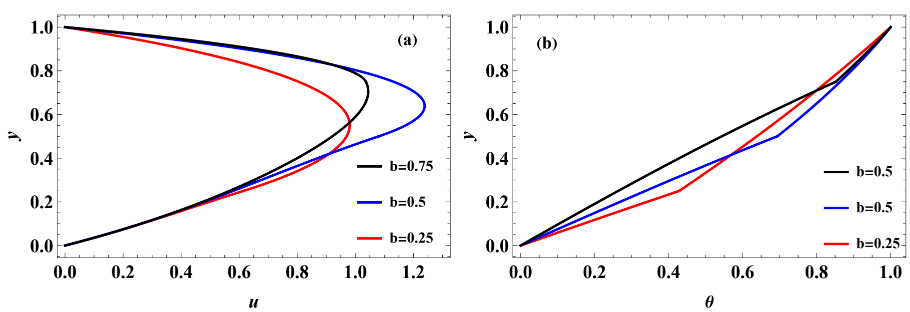

FIGURE 4. Effect of width parameter on velocity and temperature profile

The shear stress at the walls can be obtained from

$$\tau_1 = \left(\frac{A_2}{\mathrm{Re}}\frac{du_1}{dy}\right)_{y=0,1} \tag{2.20}$$

$$\tau_2 = \left(\frac{A_2}{\beta_{nf}\,\mathrm{Re}}\frac{du_2}{dy}\right)_{y=0,1} \tag{2.21}$$

The rate of heat transfer is given by:

$$Nu = \left(\frac{\partial \theta_1}{\partial y}\right)_{y=0,1} + \varepsilon_* e^{it}\left(\frac{\partial \theta_2}{\partial y}\right)_{y=0,1} \tag{2.22}$$

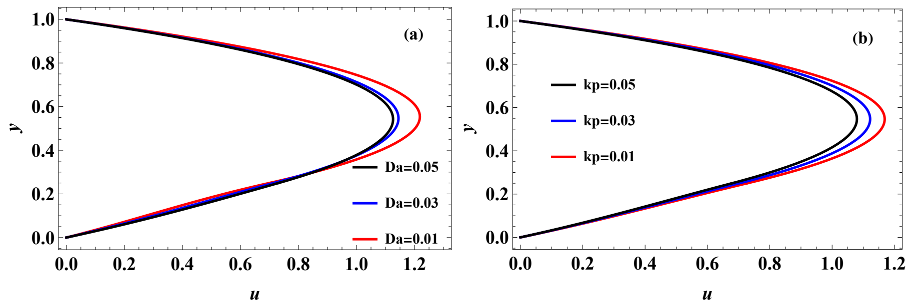

FIGURE 5. Effect of Darcy number and permeability on velocity profile

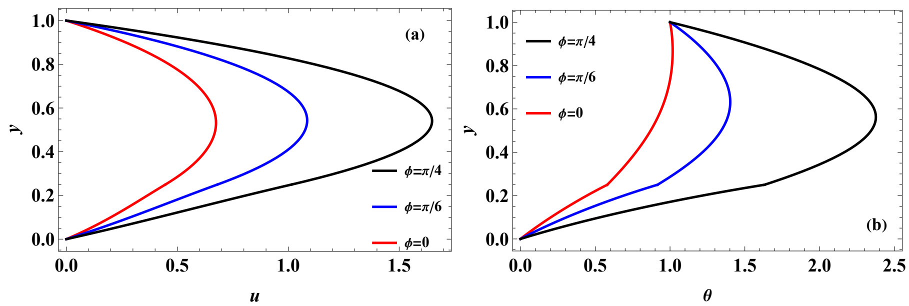

FIGURE 6. Effect of angle of inclination on velocity and temperature profile

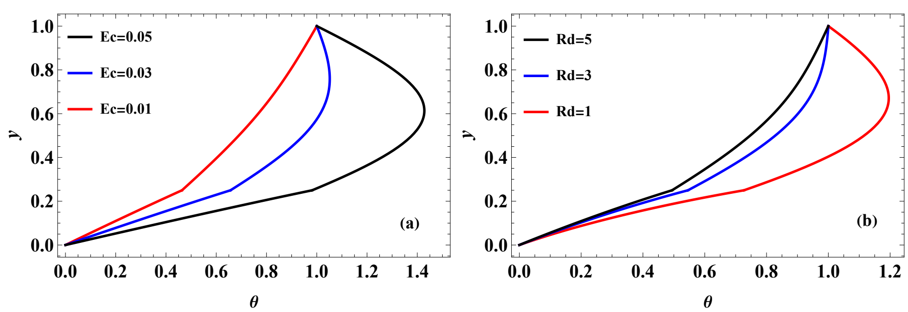

FIGURE 7. Effect of Ec and Rd parameters on temperature profile

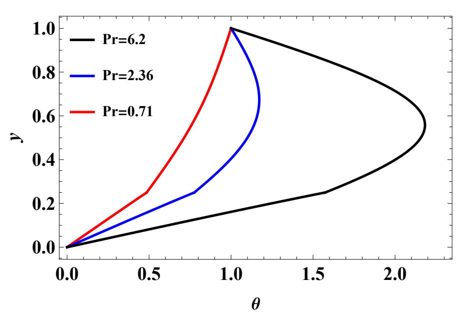

FIGURE 8. Effect of Prandtl number on temperature profile

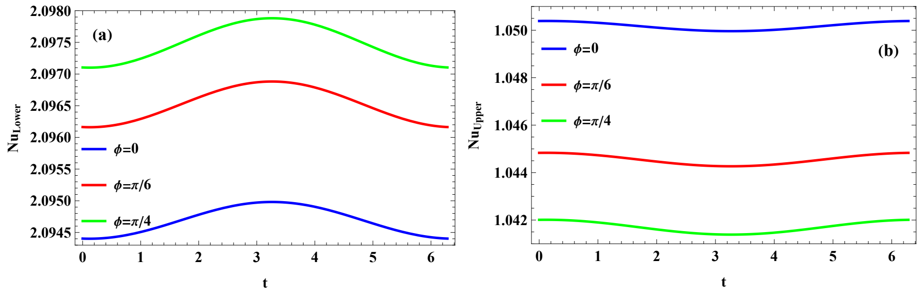

FIGURE 9. Effect of angle of inclination on Nusselt number at lower and upper walls

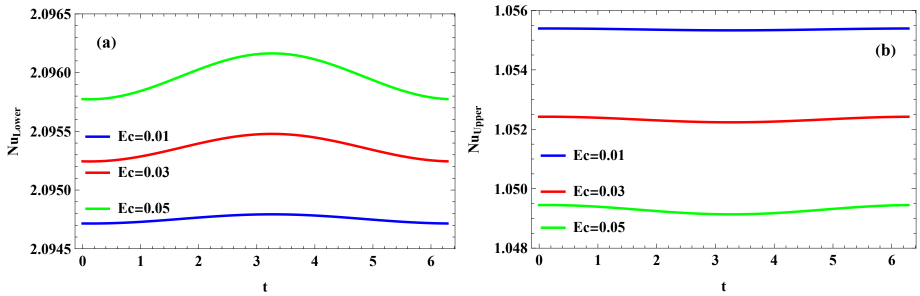

FIGURE 10. Effect of Eckert number on Nusselt number at lower and upper walls

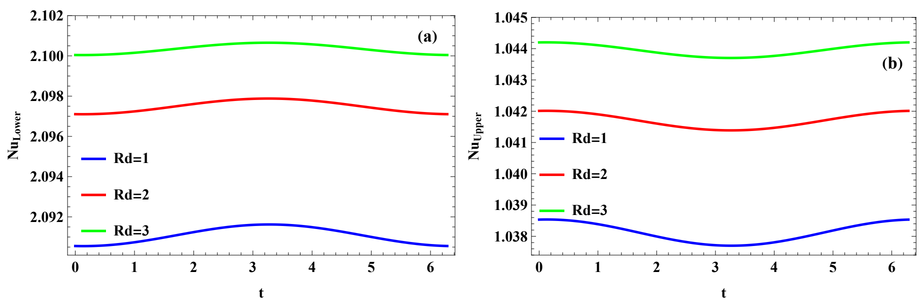

FIGURE 11. Effect of Radiation parameter on Nusselt number at lower and upper walls

3. RESULTS AND DISCUSSION

In the presence of thermal radiation and magnetic field on two-immiscible fluid flow in a porous space with water-based nanoliquid keeping two distinct nanoparticles, aluminium oxide and copper have been studied in the present study. The results are given graphically in Figs. 2-8 for velocity and temperature distributions using fixed values of $Ps = 2.5$, $Po = 2$, $R = 2$, $Gr = 1$, $M_1 = 1$, $M_2 = 2$, $k_nf = 2$, $Rd = 1$, $Pr = 0.71$, $Ec = 0.1$, $b = 0.25$, $\alpha_{nf} = 1.3834$, $R = 0.1$, $\beta_{nf} = 1$, $H = 2$, $Da = 0.05$, $kp = 2$. The governing equations for velocity and temperature were solved using the RK 4th-order method using the shooting technique. The influence of different physical phenomena on the velocity and temperature of the liquid has been discussed. The significant impact of both the Al_2O_3-water, and

Table 1. Variation of Shear stress

		M_1, M_2			D_a			ϕ		
Region	b	(0,0)	(1,2)	(2,4)	0.01	0.03	0.05	0	$\pi/6$	$\pi/4$
LR	0.25	2.097	2.098	2.096	2.07	2.061	2.059	2.072	2.063	2.059
UR		1.040	1.041	1.044	3.064	3.048	3.044	1.024	0.997	0.984
LR	0.5	1.724	1.725	1.726	1.676	1.668	1.666	1.699	1.676	1.666
UR		0.871	0.872	0.874	0.821	0.813	0.811	0.850	0.824	0.811
LR	0.75	1.455	1.456	1.458	1.400	1.394	1.393	1.434	1.406	1.393
UR		0.706	0.696	0.694	7.721	8.365	9.009	0.730	0.706	0.694

Cu-water in lower and upper region are discussed.

Figs. 2(a) and 2(b) show the impact of the Hartmann number on the velocity and temperature of the nanofluids. From the figures, one can observe that when a magnetic field is applied to both types of nanofluids, a Lorentz force will be induced. This force works opposite to the flow direction, slowing down the velocity and temperature of the liquid flow. Also, the flow distribution and temperature boundary layers get thinner as the magnetic field gets stronger. Since Al_2O_3 is less dense than Cu, the liquid flow field containing Al_2O_3 is faster than the velocity of Cu, with the base fluid being water, respectively.

Figs. 3(a) and 3(b) represent the impact of Gr on velocity and temperature profiles. Fig. 3(b) elucidates that the temperature of the liquid is enhanced when the Gr increases. This indicates that temperature increases in Region I and then exhibits parabolic behaviour in Region II as the temperature increases. A rise in the value of Gr increases the species buoyancy force, which increases the fluid's temperature and velocity. Since Gr defines the ratio between buoyancy to viscous forces. However, the temperature enhancement in water with Cu is relatively large. It is noticed from the Figs. 4(a) and 4(b), that as the width parameter increases, the velocity of the liquid oscillates, and more velocity of the nanofluid is at the upper region of the channel. When the width parameter increases, the temperature of the liquid flow decreases. From Fig. 5(a), it can be noticed that the liquid in the upper region has more temperature. As the Darcy number increases, the viscosity of the liquid can increase, but the permeability stays the same or changes slowly. This makes the flow rate go up, which makes the velocity rise. However, the region containing Al_2O_3 has higher velocity when compared to the region filled with Cu, as seen in Fig. 5(a). Fig. 5(b) elucidates that as the permeability ratio increases, the velocity falls. This means that the medium offers more resistance to flow. Figs. 6(a) and 6(b) show that both the velocity and temperature of the liquid increase as the angle of inclination increases because the driving force working on the fluid gets stronger. The liquid that contains copper nanoparticles has more velocity compared to the region filled with aluminium oxide nanoparticles, as illustrated in Figs. 6(a) and 6(b). As Ec increases, the viscous dissipation in the flow causes the temperature to increase rapidly, which also thickens the layer of the thermal boundary that is shown in Fig. 7(a). Fig. 7(b) elucidates that as Rd increases, the temperature of the liquid goes down because radiation slows down the Nusselt number. Fig. 8 elucidates that as Pr increases, the liquid temperature increases due to the fluid being more diffusive. The thermal diffusivity of a liquid tells us how fast heat can move through the liquid.

As the angle of inclination enhances at the channel of the lower wall, the Nu also increases. Whereas the reverse trend can be noticed at the channel of the upper wall, which can be seen in Figs. 9(a)-9(b). Figs. 10(a) and 10(b) represent the variation of Ec with Nu at both channel walls, respectively. With the rise in the Eckert number, it is noticed that the Nusselt number is enhanced on both channel walls. We observed from the Figs. 11(a)-11(b), that the Nusselt number in both channel walls increases as the radiation parameter increases. This observation is due to the decreasing thickness of the boundary layer with a rise of the parameter.

The numerical results for skin friction distribution are depicted with various pertinent parameters ($b = 0.25, 0.5, 0.75$) at both channel walls and are shown in Table 1. One can observe that as Da values increase, the stress distribution at both walls reduces. The stress distribution goes down as the angle of inclination goes up. It is noticed that both the channel walls have more shear stress when the Hartmann number increases.

4. Conclusion

In this investigation, the model of immiscible liquid flow inside an inclined porous space with an oscillatory pressure gradient has been explored. The influence of viscous dissipation, Darcy dissipation, and ohmic heating has been accounted in the model. The liquid in region-I contains aluminium oxide, while in region-II, copper is suspended as nanoparticles, keeping the base fluid as water. The key outcomes of the present study are as follows: When the Darcy number increases, the velocity of the liquid enhances, and a reverse trend is observed when the ratio of permeability increases. As the angle of inclination increases, both the velocity and temperature of the liquid are enhanced. When Ec increases, the Nusselt number increases at the lower wall, and a reverse trend is observed in the upper wall of the channel. Skin friction distribution on both channel walls increases when the strength of the magnetic field increases.

References

1. Abbas. A, Jeelani. M. B, & Alharthi. N.H. (2022). Darcy–Forchheimer relation influence on MHD dissipative third-grade fluid flow and heat transfer in porous medium with joule heating effects: A numerical approach. Processes. May 4;10(5):906. https://doi.org/10.3390/pr10050906
2. Bala Anasuya, J. and Srinivas, S, (2023). Heat transfer characteristics of magnetohydrodynamic two fluid oscillatory flow in an inclined channel with saturated porous medium. Proceedings of the Institution of Mechanical Engineers, Part E: Journal of Process Mechanical Engineering, p.09544089221146364. https://doi.org/10.1177/09544089221146364

3. Choi S.U.S, (1995) Enhancing thermal conductivity of fluids with nanoparticles: The Proc.1995 ASME Int. Mech. Eng. Congr. Expo, San Francisco, USA, ASME, FED 231/MD 66, pp.99–105.
4. Chon. C.H, Kihm.K.D, Lee.S.P, & Choi.S.U.S, (2005) "Empirical correlation finding the role of temperature and particle size for nanofluid (Al2O3) thermal conductivity enhancement." Appl. Phys. Lett., 87(15), 153107-1531. https://doi.org/10.1063/1.2093936
5. Das.S.K, Choi.S.U.S, & Patel. H.E, (2006) Heat Transfer in Nanofluids-A Review, Heat Transf. Eng. 27 (10), pp.3–19. https://doi.org/10.1080/01457630600904593
6. Eastman.J.A, Choi. S. U. S, Li. S, Thompson. L.J, & Lee. S, (1996) "Enhanced thermal conductivity through the development of nanofluids. Fall Meeting of the Materials Research Society (MRS), Boston, USA.
7. Evenhuis. C. J, & Haddad. P.R, (2009) Joule heating effects and the experimental determination of temperature during CE. Electrophoresis. Mar;30(5):897-909. https://doi.org/10.1002/elps.200800643
8. Goyal, K. and Srinivas, S., (2023). Entropy generation analysis for hydromagnetic two-layered pulsatile immiscible flow with Joule heating and first-order chemical reaction. Case Studies in Thermal Engineering, 47, p.103046 https://doi.org/10.1016/j.csite.2023.103046
9. Goyal, K. and Suripeddi, S., (2023). A Note on Two-Fluid Starting Flow in a Porous Spaced Channel with a Magnetic Field. CFD Letters, 15(9), pp.136-151. https://doi.org/10.37934/cfdl.15.9.136151
10. A Problem with periodic boundary conditions for the non-fourier heat equation. Gulf Journal of Mathematics, Vol.15, 2, 1-14, 2023. https://doi.org/10.56947/gjom.v15i2.1373
11. Wang. X.Q, & Mujumdar. A.S, (2007) Heat transfer characteristics of nanofluids: a review, Int. J.Therm. Sci. 46, pp-1-19. :10.1016/j.ijthermalsci.2006.06.010
12. Kuznetsov. A.V, & Nield. D.A, (2010) Natural convective boundary-layer flow of a nanofluid past a vertical plate. International Journal of Thermal Sciences. Feb 1;49(2):243-7. https://doi.org/10.1016/j.ijthermalsci.2009.07.015
13. Malvandi. A, Safaei. M.R, Kaffash. M. H, & Ganji. D.D, (2015) MHD mixed convection in a vertical annulus filled with Al2O3–water nanofluid considering nanoparticle migration. Journal of Magnetism and Magnetic Materials. May 15;382:296–306. http://dx.doi.org/10.1016/j.jmmm.2015.01.060
14. Padma Devi, M., and Srinivas, S. (2022). Thermal characteristics on two immiscible fluid flows in a porous space with time dependent pressure gradient. Proceedings of the Institution of Mechanical Engineers, Part E: Journal of Process Mechanical Engineering, 236(6), 2480-2490. https://doi.org/10.1177/09544089221096569
15. Sivashanmugam. P, (2012). Application of nanofluids in heat transfer. An overview of heat transfer phenomena. Oct 31;16. 10.5772/52496
16. Sheikholeslami. M, Gorji-Bandpy. Ellahi. M. R, & Zeeshan.A, (2014) Simulation of MHD CuO–water nanofluid flow and convective heat transfer considering Lorentz forces, J. Mag. Magn. Mater. 369, 69-–80. https://doi.org/10.1016/j.jmmm.2014.06.017
17. Swain.B,K, Parida. B. C, Kar. S, & Senapati.N, (2020) Viscous dissipation and joule heating effect on MHD flow and heat transfer past a stretching sheet embedded in a porous medium. Heliyon. Oct 1;6(10). https://doi.org/10.1016/j.heliyon.2020.e05338
18. Ur Rasheed. H, AL-Zubaidi.A, Islam.S, Saleem.S, Khan. Z, & Khan. W, (2021). Effects of Joule heating and viscous dissipation on magnetohydrodynamic boundary layer flow of Jeffrey nanofluid over a vertically stretching cylinder. Coatings. Mar 19;11(3):353. https://doi.org/10.3390/coatings11030353
19. Wang, Y., Wang, S., Xue, S., & Adhikary, D. (2015). Numerical modeling of porous flow in fractured rock and its applications in geothermal energy extraction. Journal of Earth Science, 26, 20-27. https://doi.org/10.1007/s12583-015-0507-1

[1] Department of Mathematics, St. Peter's Engineering College, Dhulapally Post, Medchal Mandal, R.R. District, Medchal, Telangana, 500100, India
Email address: padmadevimedisetti@gmail.com

[2] Department of Mathematics, VIT-AP University, Amaravati, Guntur, Andhra Pradesh, 533327, India.
Email address: komalgoelresearch@gmail.com, srinusuripeddi@gmail.com, satyabadeti1980@gmail.com